

# Non-proportionality analysis of multiaxial fatigue stress histories in trailing edge adhesive joints of wind turbine rotor blades

Claudio Balzani<sup>1</sup> and Pablo Noever Castelos<sup>1</sup>

<sup>1</sup>Leibniz University Hannover, Institute for Wind Energy Systems, Appelstr. 9A, 30167 Hannover, Germany

**Correspondence:** Claudio Balzani (research@iwes.uni-hannover.de)

**Abstract.** Wind turbine rotor blades are exposed to complex multiaxial stress states due to the aero-(hydro-)servo-elastic behaviour of the turbine. The dynamic response of rotor blades can result in non-proportional stress histories in the adhesive joints. These are not properly considered in current design guidelines and standards. However, knowledge about the degree of non-proportionality is crucial for choosing an appropriate fatigue analysis framework.

5 This paper investigates the degree of non-proportionality of three-dimensional stress histories in trailing edge adhesive joints of wind turbine rotor blades. For the quantification of non-proportionality, the concept of so-called non-proportionality factors is utilized. Existing approaches show weaknesses for the application to adhesives. Hence, a novel non-proportionality factor is introduced in this work that combines two formulations from literature. After a concise verification, it is applied to analyze the trailing edge adhesive joints of three different blade designs in the framework of a numerical comparative study.

10 The results do not reveal any correlation between the degree of non-proportionality and the blade size. General conclusions are hard to draw, as the blade response does not only depend on the turbine size, but also on the blade design philosophy. ~~However, each blade~~ Each blade in this study shows significant degrees of non-proportionality that ~~should not be neglected in fatigue damage analyses~~ may be important to take into account in a fatigue analysis.

## 1 Introduction

15 During a wind turbine's lifetime, rotor blades and their adhesive joints are subjected to multiaxial stress states. According to current design guidelines for wind turbine rotor blades (e.g., DNV GL, 2015), fatigue analyses of adhesive joints have to take into account these multiaxial stress states. However, these regulations lack of clear descriptions of associated analysis procedures. Picking up ~~longterm research goals formulated by van Kuik et al. (2016); van Kuik and Peinke (2016)~~ research challenges formulated by van Kuik et al. (2016); van Kuik and Peinke (2016); Veers et al. (2019, 2023), the question arises if  
20 failure of adhesive joints exposed to multiaxial fatigue loads can be well predicted. A thorough understanding of the nature of stress states in the adhesives throughout their lifetime is inevitable for choosing (or developing) an appropriate fatigue analysis framework and for designing validation test methods.

Fatigue analyses may ~~follow~~ be based on global stress-strength relationships, ~~see e. g. Beltrami (1885); von Mises (1913); Schleicher (1913)~~ or similar approaches. These take into account the complete three-dimensional stress tensor and (Beltrami, 1885; von Mises, 1913; Schleicher, 1913).

25 Some of these have already been applied to rotor blade adhesives (Noever Castelos and Balzani, 2016a; Antoniou et al., 2018;

Eder et al., 2020) ~~-. This approach translates and take into account the coupling between different three-dimensional stress components. They translate~~ the stress tensor to the scalar-valued global equivalent stress, which is easy to handle in a ~~classical~~ ~~rainflow counting scheme cycle counting scheme such as rainflow counting~~ (Endo et al., 1974; Downing and Socie, 1982; Rychlik, 1987; Lee and Tjhung, 2012). However, the transition from an engineering stress space to an equivalent stress space  
30 must thoroughly consider potential tension-compression asymmetries, which are present in epoxy-based adhesives (Wentingmann et al., 2022). Moreover, the method is only valid for proportional stress histories (Kuhn et al., 2023). In this case, the major principal stress direction is not changing with time, but the amplitude may vary (Stephens et al., 2001).

~~However, the~~ ~~The~~ loads acting on rotor blades are strongly dynamic (Söker, 2013; Liu et al., 2017) and non-linear (Manolas et al., 2015; Noever Castelos and Balzani, 2016b). E.g., lead-lag bending (also known as edgewise bending), which is gov-  
35 erned by the rotor blades' inertia, is mostly deterministic and harmonic with an excitation frequency of the rotor rotation speed and multiples thereof. On the other hand, fore-aft bending (also called flapwise bending) is triggered by aerodynamic forces. These are more stochastic in the time domain, due to the turbulent wind inflow (White and Musial, 2004). Speaking more clearly, the normal stress in spanwise direction is dominant in trailing edge adhesive joints, and is mainly caused by lead-lag bending (Noever Castelos and Balzani, 2016a). The fore-aft bending contributes to the normal stress to a minor extent due  
40 to a smaller offset from the related principal bending axis (Bak et al., 2013), but is, besides torsion, predominantly responsible for shear stresses in the trailing edge adhesive joint. Since the ~~lead-leg~~ ~~lead-lag~~ and the fore-aft loads are generally not in phase, the share of each stress component in the three-dimensional stress tensor will change in time. Consequently, the ~~orientation of the major principal stress changes~~ ~~orientations of the principal stresses change~~ as well, which, by definition ~~(e.g., Socie and Marquis, 2000)~~ ~~(e. g., Socie and Marquis, 2000)~~, results in non-proportional stress time series. These cannot be  
45 captured by global equivalent stress approaches (Fatemi and Shamsaei, 2011; Kuhn et al., 2023).

A physically more meaningful way is to apply the critical plane approach (Socie and Marquis, 2000; de Castro and Meggiolaro, 2016; Deng et al., 2022, 2023). Therein, the damage calculation is restricted to the plane on which a physical crack will appear, which is called the critical plane. Such concepts evaluate local equivalent stress functions that are formulated on  
50 the critical plane and take into account the normal stress perpendicular and the two shear stresses (or the resulting shear stress) parallel to such plane. However, the orientation of the critical plane may change with time, which is linked to the orientation change of the first principal stress (Anes et al., 2014). It is thus not known *a priori* in non-proportional stress histories and needs to be a result of the fatigue analysis. A computationally efficient method for the determination of the critical plane orientation was proposed by ~~?~~ ~~Wentingmann et al. (2018)~~.

It may be obvious to believe that the use of global equivalent stresses for non-proportional time series is conservative, as  
55 damage is accumulated on all effective planes. The result should therefore be significantly greater damage than with the critical plane approach, where the damage is only accumulated on the actual critical plane. However, it has been experimentally proven for an epoxy resin-based rotor blade adhesive at coupon level that neutral material behaviour occurs (Kuhn et al., 2023). This means that the fatigue life does not depend on the degree of non-proportionality (Sonsino, 2020). This behaviour can be reproduced with the critical-plane approach, but not with the global approach. On the contrary, it could be shown that the  
60 fatigue damage in the case of the global equivalent stress ~~approach~~ ~~approach~~ is not higher for increasing non-proportionality,

but significantly lower (Kuhn et al., 2023). In this respect, the global approach not only incorrectly predicted the basic fatigue behaviour (i.e. i.e., it did not capture the neutral behaviour), but also significantly overestimated the fatigue life. The prediction was therefore substantially non-conservative.

Consequently, the choice of an appropriate fatigue analysis concept depends on the degree of non-proportionality. It is thus important to gain deep knowledge of the characteristics of stress histories in rotor blade adhesive joints and to.

## 1.1 Quantification of non-proportionality

To quantify the degree of non-proportionality in the stress histories, which so-called *non-proportionality factors* denoted by  $f_{NP}$  are commonly used. These are scalar-valued magnitudes with values between 0 (for purely proportional stress histories) and 1 (for purely non-proportional stress histories). Socie and Marquis (2000) presented a selection of approaches to calculate a non-proportionality factor. They have in common that each time instance in a stress time series is plotted in the stress domain. The conglomeration of all these points forms a body in the six-dimensional stress space if the whole stress tensor is considered, and reduces to less dimensions if stress components are neglected.

One approach is to consider the non-proportionality factor as the aspect ratio of a minimum size convex surface surrounding this body. This convex surface is an ellipsis in the two-dimensional case. The concept is visualised for three different artificial 2D cases in Figure 1, where the shear stress  $\tau_{xy}$  is combined with the normal stress  $\sigma_x$ . The convex hull method is easy to apply in the 2D stress space. However, it becomes more complicated with increasing dimension, as one needs to consider ellipsoids in the 3D stress space or hyper-ellipsoids in the general case (Zouain et al., 2006). Besides, the non-physical and rather geometric nature of this method is linked with a loss of information on the cyclicity of the stress time series due to the generalizing hull, and can lead to poor predictions of  $f_{NP}$  depending on the load path complexity (Meggiolaro and de Castro, 2012).

Kanazawa et al. (1979) presented a different approach estimating  $f_{NP}$  by means of a rotation factor, which is defined by the inverse of the ratio between the maximum shear strain range and the shear strain with an orientation of  $45^\circ$  to the maximum shear strain range. This factor represents the ellipticity of the load path in the bi-axial  $\tau_{xy}$ - $\sigma_x$  stress space and depends on both the phase angle and the amplitude (Socie and Marquis, 2000). Following a similar idea, Itoh et al. (1995) evaluated the temporal integral of the product of the largest principal strain in each time instance (denoted by  $\varepsilon_1$ ) and the angular deviation between  $\varepsilon_1$  and its time-related maximum in the time series. This approach, originally introduced for 2D load paths, was later extended to a 3D representation (Itoh et al., 2013), but is not applicable for the general six-dimensional case.

Bishop (2000) introduced an analogy to mass moments of inertia. Using Mandel notation, the state of stress for each time instance was mapped as a point in the six-dimensional stress space. The rectangular moment of inertia (RMOI) matrix of the accumulation of these points for a complete time series was calculated with respect to the mean stress. The non-proportionality factor was then defined by the square root of the ratio between the largest and second-to-largest eigenvalue of the RMOI matrix. Meggiolaro et al. (2016) concluded the following drawbacks of this approach: (i) The Bishop non-proportionality factor is formulated in the stress space instead of a more appropriate plastic strain space; (ii) the 6D formulation implicitly assumes an influence of the hydrostatic pressure, which is wrong for materials with pressure-insensitive yield functions; (iii) the rectangular moments of inertia are calculated with respect to a mean, which produces errors for certain load paths;

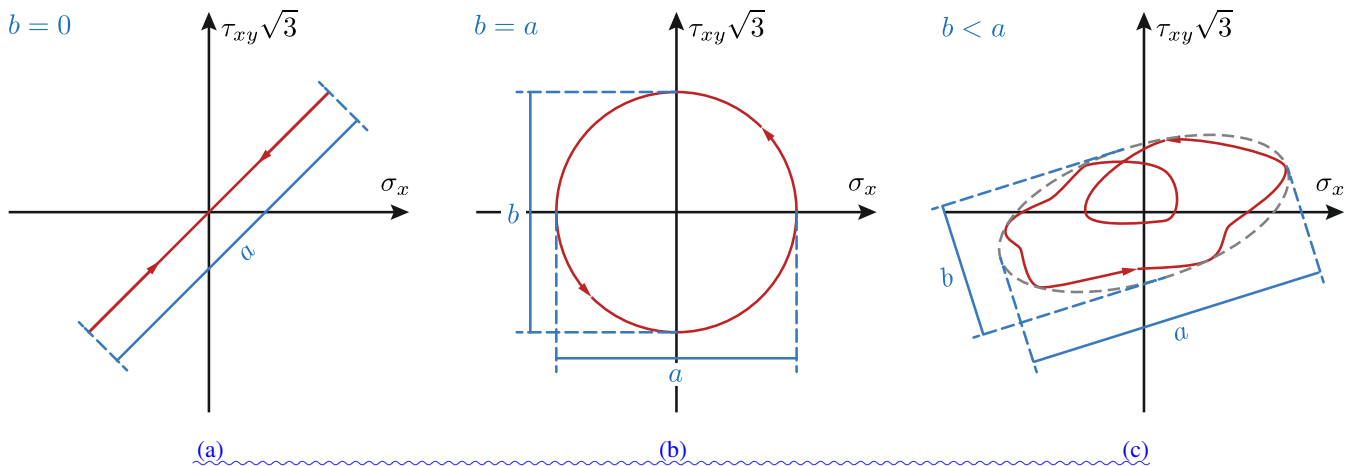


**Figure 1.** Minimum size convex hull surrounding the body spanned by the stress states in each time instance of a stress time series in the two-dimensional case (reproduced from Socie and Marquis (2000)): (a) proportional stress time series with  $f_{NP} = \frac{b}{a} = 0$  (expressed by a straight line, i. e.,  $b = 0$ ); (b) stress time series with  $90^\circ$  phase shift and  $f_{NP} = \frac{b}{a} = 1$  (expressed by a circle, i. e.,  $a = b$ ); (c) arbitrary time series with  $0 < f_{NP} < 1$ , as  $b < a$ .

95 (iv) the Bishop non-proportionality factor gives wrong results for tension-torsion load paths, where it describes a circle in a  $\sigma_{ii}$  versus  $\sqrt{2}\sigma_{jk}$  diagram, with  $j \neq k$ , and not for the well-known  $90^\circ$  phase shift with a circle in the  $\sigma_{ii}$  versus  $\sqrt{3}\tau_{jk}$  diagram. Meggiolaro and de Castro (2014) represented the stresses in a 5D deviatoric subspace and calculated the RMOI matrix of the resulting 5D stress path independently of a mean. In this way, the aforementioned drawbacks were eliminated. This approach showed good agreement with experimental results for metals (Meggiolaro and de Castro, 2014). However,

100 polymers are sensitive to the hydrostatic pressure (Adams, 2005; Amos Gilat et al., 2005; Hu et al., 2003; Beber et al., 2017). A combination of the approaches from (Bishop, 2000; Meggiolaro and de Castro, 2014) is thus proposed in this work to adapt the non-proportionality factor to a polymeric adhesive.

## 1.2 Fatigue in trailing edges of wind turbine rotor blades

A variety of damage types is observed in rotor blades in operational settings (Katsaprakakis et al., 2021; Boopathi et al., 2022)

105 The following ones are found to occur predominantly on trailing edges: Longitudinal cracks along the adhesive joint and transverse cracks within the adhesive and the surrounding laminate structures (Ataya and Ahmed, 2013).

The longitudinal cracks can manifest as a cohesive crack through the adhesive or as a detachment of the adhesive from the substrates. In some cases, these phenomena may occur as a combination of both possibilities. Such cracks are caused, for instance, by peel stresses in the adhesive resulting from a pumping motion of the trailing edge panels (Eder et al., 2014)

110 which is associated with the warping of cross-sections in the cross-sectional plane and is also called *blade breathing* (Balzani and Gebauer, 2023). To characterise the peel strength and toughness, tests were conducted at the coupon or small-scale structural level (Eder and Bitsche, 2015; Fan et al., 2024). Rosemeier et al. (2020) put forth a pragmatic methodology for evaluating

115 peel stresses in rotor blade adhesive joints. In addition to blade breathing, geometrically non-linear undulating deformations of the trailing edge associated with the transition to buckling may occur in a region around the maximum chord length. Such deformation can also result in the formation of longitudinal cracks in the trailing edge adhesive joint due to a mixture of shear and peel stresses. This type of damage was observed in full-scale blade tests and could be reproduced in numerical simulations (Haselbach and Branner, 2015; Haselbach et al., 2016; Haselbach and Branner, 2016; Haselbach, 2017).

120 Subsequently, a series of sub-component tests were conducted, in which trailing edge segments were subjected to eccentric axial compression, which was representative for trailing edges in a blade, in order to induce buckling (Lahuerta et al., 2018; Chen et al., 2019). The tests revealed that, as a consequence of the trailing edge buckling, debonding in the adhesive joint and subsequent cracks in the trailing edge panels occurred, mostly on the suction side and particularly in the sandwich core. Numerical simulations using the finite element method could represent the damage behaviour observed during most of the tests (Lahuerta et al., 2018; Chen et al., 2019a, b). Ashish et al. (2023) have proposed an analytical method to describe debonding of a trailing edge adhesive joint under simplifying assumptions, which is useful for quick assessments without detailed finite element simulations. However, all the  
125 aforementioned studies on sub-component level were limited to static loads.

Transverse cracks were observed in operating wind turbines (Ataya and Ahmed, 2013) and in full-scale rotor blade tests (Rosemeier et al., 2022b). In terms of fatigue, the majority of analysis was conducted numerically (Rosemeier et al., 2019a, b). It can be concluded that these cracks are a consequence of the predominant occurrence of cyclic longitudinal strains in the trailing edge, which results in the generation of high longitudinal normal stresses in the adhesive. These stresses exceed the  
130 fatigue-related load-carrying capacity of the adhesive over time. However, it should be noted that thermal residual stresses can also exert a significant influence on the formation of cracks. It has been demonstrated that the exclusion of thermal residual stresses can result in an underestimation of fatigue damage by up to 30-40% (Antoniou et al., 2020). It was reasonably deduced that the thermal residual stresses are responsible for the majority of the mean stress, while the mechanical loads resulting from turbine operation are responsible for the majority of the stress amplitudes (Rosemeier et al., 2022b). Furthermore, it was  
135 highlighted that in exceptional circumstances, thermal residual stresses can result in the formation of transverse cracks even during the manufacturing process (Rosemeier et al., 2022a). In the aforementioned publications, however, the thermal residual stresses were calculated under simplifying assumptions. Relaxation for instance, which has the potential to significantly reduce the thermal residual stresses, necessitates intricate characterisation and has yet to be addressed. Furthermore, it is not possible to determine thermal residual stresses directly through experimentation; instead, they must be recalculated based on the  
140 diversions of deformation measurements. This was demonstrated in coupon experiments (Jørgensen et al., 2019). However, the corresponding deformations of a rotor blade trailing edge are likely to be very small and therefore challenging to measure, which complicates the validation of thermal residual stresses in a full-scale rotor blade structure.

The investigations into the occurrence of transverse cracks, as previously referenced, were conducted utilising global equivalent stresses in order to account for the interactions between stress components. As previously stated, these methods do  
145 not sufficiently address non-proportionality in the stress time series. The topic of non-proportional fatigue in wind turbine rotor blades has been explored by several researchers (Vassilopoulos, 2013; Hu et al., 2016; Rubiella et al., 2018; Hu et al., 2020). However, the subject has not been extensively investigated yet. The aforementioned publications are limited in scope, focusing

150 exclusively on non-proportional fatigue in the composite laminate components of wind turbine blades and neglecting fatigue damage in adhesive joints. There is very little literature that specifically investigates non-proportional fatigue in trailing edge adhesive joints (Balzani, 2018; Wentingmann, 2018). However, a comprehensive analysis of the non-proportionality characteristics in the adhesive joint was not conducted. To the best of the authors' knowledge, there is no existing publication that studies the degree of non-proportionality in the stress time series of a trailing edge adhesive joint.

### 1.3 Research objective

155 The objective of this study is to address the aforementioned gap in knowledge. The underlying hypothesis is that a significant amount of non-proportionality can occur in stress time series of trailing edge adhesive joints. The aim is not to study the fatigue damage itself, but to thoroughly analyze the stress time series that serve as the basis for calculating the fatigue damage in adhesive joints and to derive an equivalent value for their lifespan. This fundamental knowledge is crucial for choosing an appropriate fatigue analysis framework during the design of wind turbine rotor blades. The overall methodology employed in this study is ~~the focus of this paper. The overall methodology followed in this work is~~ outlined in the following section.

## 160 **2 Methodology**

The aim of this work is to study the degree of non-proportionality in fatigue-related stress time series in trailing edge adhesive joints of wind turbine rotor blades. The fatigue analysis itself or the choice of a fatigue analysis framework based on the non-proportionality analysis are not subject of this paper and will be addressed in future work.

165 employed. ~~Some of the formulations available in literature are briefly reviewed. The mathematical formulation of the approach used in this study is derived~~ in section 3. ~~As all of them show weaknesses for adhesive joints, a~~ A novel non-proportionality factor is proposed that combines two existing formulations. The main benefit is that the new formulation accounts for the dependency of the fatigue behavior of an epoxy-based adhesive on the hydrostatic stress state. The new non-proportionality factor is verified using numerical examples from literature.

170 Application examples are then selected in section 4 for which the analyses are carried out. Three blades are considered: (i) the 86 m DTU 10 MW Reference Wind Turbine Blade (Bak et al., 2013), (ii) the 80 m IWES IWT-7.5-164 Reference Wind Turbine Blade (Popko et al., 2018) from the *Smart Blades* project (Teßmer et al., 2016), and (iii) the 20 m Demonstration Blade (Bätge, 2016) from the *SmartBlades2* project (called *SB2-DemoBlade* in the following). The latter blade has a pre-sweep in the rotor area for introducing a geometrical bend-twist coupling. The sweep is supposed to introduce a higher portion of shear stresses in the adhesive due to torsion and thus a higher degree of non-proportionality. The blades were ~~chosen as selected~~ because the first two are similar in size and the third is significantly smaller. In this way we can compare different blade sizes while taking into account different design philosophies.

The methodology for the calculation of non-proportionality factors consists of three steps: (i) Determination of loads through turbine simulations, (ii) calculation of 3D stress tensors in the adhesive, and (iii) evaluation of the degree of non-proportionality

180 by means of the non-proportionality factor. The loads analyses are limited to the *normal operation* design load case. The extracted blade loads, which are internal forces and moments according to beam theory, are transformed to 3D stress time series in the adhesive, as these are the required input for the non-proportionality factor. The transfer was done via a 3D finite element [model simulations](#) of each blade and application of external loads according to a methodology that has been published previously (Noever Castelos and Balzani, 2016b). The stress time series are used to calculate the non-proportionality factor in  
185 each finite element representing the adhesive at different wind speeds.

The distribution of the non-proportionality factor along the blade is then investigated as a function of the wind speed. An attempt is made to correlate the degree of non-proportionality with the stress time series in elements representing the adhesive. The distribution of the non-proportionality factor in the cross-sectional direction are also discussed, and a wind velocity-weighted mean non-proportionality factor is introduced for comparison between the different blades. An attempt to derive  
190 conclusions from the comparisons is made at the end of the paper.

### 3 [Quantification Mathematical formulation of the non-proportionality in multiaxial stress histories factor](#)

[Socie and Marquis \(2000\)](#) briefly present a selection of approaches to calculate a so-called [For the quantification of non-proportionality we follow the concept of a scalar-valued non-proportionality factor  \$f\_{NP}\$](#) . ~~These have in common that a data point is plotted in the stress domain for each time instance of the stress time series. The conglomeration of all these points forms a body in the six-dimensional stress space<sup>1</sup>. The first approach considers  $f_{NP}$  as the aspect ratio of a minimum size convex surface surrounding this body, which would be an ellipsis in [outlined in the introduction. We start the derivation of a two-dimensional case. This concept is visualised for three different artificial 2D cases in Figure ??, where the shear stress  \$\tau\_{xy}\$  is combined with the normal stress  \$\sigma\_x\$ .](#)~~

(a) ————— (b) ————— (c) Minimum size convex hull surrounding  
200 the body spanned by the data points of stress instances in the stress time series in the two-dimensional case (reproduced from Socie and Marquis (2000)): (a) proportional stress time series with  $f_{NP} = \frac{b}{a} = 0$  (expressed by a straight line, i. e.  $b = 0$ ); (b) stress time series with 90° phase shift and  $f_{NP} = \frac{b}{a} = 1$  (as  $a = b$ ); (c) arbitrary time series with  $0 < f_{NP} < 1$  for  $a > b$ .

This convex hull method is easy to apply in the 2D stress space. However, it becomes more complicated with increasing dimension, as one needs to compute ellipsoids in the 3D stress space or hyper-ellipsoids in the general case, as [Zouain et al. \(2006\)](#)  
205 discuss in detail. Besides, the non-physical and rather geometric nature of this method is linked with a loss of information on the cyclicity of the stress time series due to the generalizing hull, and can lead to poor predictions of  $f_{NP}$  depending on the load path complexity ([Meggiolaro and de Castro, 2012](#)). [Kanazawa et al. \(1979\)](#) presented a different approach estimating  $f_{NP}$  by means of a rotation factor, which is defined by

$$f_{NP} = \frac{\text{Shear strain } 45^\circ \text{ to maximum shear strain range}}{\text{Maximum shear straining range}}.$$

<sup>1</sup>The stress space is six-dimensional only if the complete stress tensor is included. It is e. g. reduced to three dimensions if only the normal stresses are considered.

210 This factor represents the ellipticity of the load path in the  $\tau_{xy}$  vs.  $\sigma_x$  biaxial stress space and depends on both the phase angle and the amplitude (Socie and Marquis, 2000). Following a similar idea, Itoh et al. (1995) integrated the product of the highest principal strain of the load path,  $\varepsilon_1$ , and its angular deviation to the maximum value of  $\varepsilon_1$ ,  $\xi$ , over the related time period  $T$  according to

$$f_{NP} = \frac{\pi}{2T\varepsilon_{1,\max}} \int_0^T \varepsilon_1(t) |\sin(\xi(t))| dt.$$

215 Herein,  $\varepsilon_{1,\max}$  denotes the maximum value of  $\varepsilon_1$  in the time series, i. e.,  $\varepsilon_{1,\max} = \max\{\varepsilon_1(t)\}$ ,  $|\cdot|$  is the norm of  $(\cdot)$ , and  $t$  is the time. This expression for 2D load paths was later extended to a 3D expression in Itoh et al. (2013). However, it is still not applicable for the general 6D case.

A different formulation was introduced by Bishop (2000) using mathematical formulation with the concept of Bishop (2000), who introduced an analogy to mass moments of inertia. Using Mandel notation, he represented the symmetric second order Mandel notation is used to replace the symmetric stress tensor, the metrics of which defined whose metric is expressed by a  $3 \times 3$  matrix, by with a six-dimensional vector  $\sigma_M \in \mathbb{R}^6$  following  $\sigma_M \in \mathbb{R}^6$  according to

$$\sigma_{3 \times 3} = \begin{pmatrix} \sigma_{11} & \sigma_{12} & \sigma_{13} \\ \sigma_{21} & \sigma_{22} & \sigma_{23} \\ \sigma_{31} & \sigma_{32} & \sigma_{33} \end{pmatrix} \Rightarrow \sigma_M = (\sigma_{11}, \sigma_{22}, \sigma_{33}, \sqrt{2}\sigma_{12}, \sqrt{2}\sigma_{13}, \sqrt{2}\sigma_{23})^T. \quad (1)$$

The state of stress at a specific point in time for a given time instance can be mapped as a point in the six-dimensional stress space. The collection of these points for a complete stress time series, i. e., the accumulation of such points for all time instances along a time series, results in a six-dimensional body, which is called referred to as stress body in the following. The rectangular moment of inertia (RMOI) matrix of the stress body is denoted by  $I \in \mathbb{R}^6$  and is calculated using the expression

$$I = \oint_{\Sigma} (\sigma_M - \bar{\sigma})(\sigma_M - \bar{\sigma})^T |d\sigma|. \quad (2)$$

Herein, the RMOI matrix is calculated with respect to the mean stress  $\bar{\sigma}$ , which is determined by the expression relationship

$$\bar{\sigma} = \frac{1}{L} \oint_{\Sigma} \sigma_M |d\sigma_M|, \quad \text{with} \quad L = \oint_{\Sigma} |d\sigma|. \quad (3)$$

230 Provided that  $|d\sigma|$  represents the Euclidean distance between two time steps,  $L$  reflects the complete Euclidean arc length of the stress path  $\Sigma$  that connects all points of the stress body in chronological order. Calculation of the  $n$  eigenvalues  $\lambda_i$  of the RMOI matrix  $I$  and sorting them in decreasing order, i. e.,  $\lambda_1 > \lambda_2 > \dots > \lambda_n$ , yields the non-proportionality factor according to Bishop (2000) defined by

$$f_{NP} = \sqrt{\frac{\lambda_2}{\lambda_1}}, \quad (4)$$

Meggiolaro et al. (2016) analysed this expression and concluded the following: (i) Equation (4) is formulated in the stress space instead of a more appropriate plastic strain space. (ii) The 6D formulation implicitly assumes an influence of the hydrostatic pressure, which is wrong for materials with pressure insensitive yield functions. (iii) The rectangular moments of inertia are calculated with respect to a mean, which produces errors for certain load paths. (iv) Equation (4) gives wrong results for tension-torsion load paths, where it describes a circle in a  $\sigma_{ii}$  versus  $\sqrt{2}\sigma_{jk}$  diagram, with  $j \neq k$ , and not for the well known  $90^\circ$  phase shift with a circle in the  $\sigma_{ii}$  versus  $\sqrt{3}\tau_{jk}$  diagram. Hence, Meggiolaro and de Castro (2014) developed a different method. Therein, see Bishop (2000). A reformulation was introduced by Meggiolaro and de Castro (2014), in which the stresses are represented in a 5D deviatoric subspace given by

$$\boldsymbol{\sigma}_{\text{dev}} = (S_1, S_2, S_3, S_4, S_5)^T, \quad (5)$$

245 where

$$S_1 = \sigma_{11} - \frac{\sigma_{22} + \sigma_{33}}{2}, \quad S_2 = \sqrt{3} \frac{\sigma_{22} - \sigma_{33}}{2}, \quad S_3 = \sqrt{3} \tau_{12}, \quad S_4 = \sqrt{3} \tau_{13}, \quad \text{and} \quad S_5 = \sqrt{3} \tau_{23}. \quad (6)$$

By describing the stresses in the deviatoric stress space the aforementioned issues are solved due to the following reasons: It represents the plastic strain space, see (i), disregards the hydrostatic component, see (ii), and a circle in the  $\sigma$  versus  $\sqrt{3}\tau$  diagram is recognized as such, see (iv). The In contrast to equation (2), the RMOI matrix  $\mathbf{I} \in \mathbb{R}^5$  of the 5D stress path  $\Sigma$  is calculated independently of a mean, cf. (iii). It and is given by the expression

$$\mathbf{I} = \frac{1}{L} \oint_{\Sigma} \boldsymbol{\sigma}_{\text{dev}} \boldsymbol{\sigma}_{\text{dev}}^T |d\boldsymbol{\sigma}|. \quad (7)$$

The non-proportionality factor  $f_{NP}$  is then calculated according to equation (4). This approach-reformulation overcomes some general deficiencies of Bishop's formulation identified by Meggiolaro et al. (2016): It represents the plastic strain space, disregards the hydrostatic component, the RMOI matrix is independent of a mean, and a circle in the  $\sigma$  versus  $\sqrt{3}\tau$  diagram is recognized as such. It thus shows good agreement with experimental results for metals (Meggiolaro and de Castro, 2014). However, polymers, such as adhesive joints made of epoxy epoxy-based adhesives considered in this study, are sensitive with respect to the hydrostatic pressure, see e.g. Adams (2005); Amos Gilat et al. (2005); Hu et al. (2003); Beber et al. (2017); (Adams, 2005; Amos Gilat et al., 2005; Hu et al., 2003; Beber et al., 2017). That is accounted for in equation (2), but not in equation (7). However, the RMOI matrix should not be related to a mean, as already mentioned because that produces errors for certain load paths. We thus redefine

$$\mathbf{I} \in \mathbb{R}^6 = \oint_{\Sigma} \boldsymbol{\sigma}_M \boldsymbol{\sigma}_M^T |d\boldsymbol{\sigma}_M|. \quad (8)$$

In the latter expression, we combine the advantages of equation (2) and equation (7) by omitting the mean stress  $\bar{\boldsymbol{\sigma}}$  and including the full stress tensor in Mandel notation in order to account for the hydrostatic pressure. Hence, the problem that a  $90^\circ$  phase shift path is not represented by a circle in the  $\sigma$  versus  $\sqrt{3}\tau$  diagram still exists. However, we assume linear elastic

**Table 1.** Stress history characteristics of the applied 20 test cases. Test cases are taken from Itoh et al. (1995) and Meggiolaro and de Castro (2014) and are plotted in Figure 2.

Characteristics of stress histories	Test case number
Proportional loading	1,6
Only two principal stress directions	1-6
Full reversed loading	2-5
Rotating principal stress direction	2,6,9-15,17
Step length	6-10
90° phase shift	15
Small principal stress direction variation	7,16
45° principal stress direction variation	18
Mean value influence	9,10,16,18,19
Random path	19,20

265 material behavior of the adhesive when transforming load time series into stress time series as described in (Noever Castelos  
and Balzani, 2016b). A plastic strain path representation is thus not necessary. The non-proportionality factor  $f_{NP}$  is still  
computed following equation (4).

~~Load history test cases used for comparison of the non-proportionality factor approaches, extracted and reproduced from  
Itoh et al. (1995) and Meggiolaro and de Castro (2014).~~

270 In order to compare the three approaches described above, 20 different synthetic stress paths are evaluated, see Figure 2.  
The choice of these paths is discussed in Itoh et al. (1995) and Meggiolaro and de Castro (2014). The characteristics of the  
underlying stress histories and the corresponding test case numbers are summarized in Table 1. The first 15 paths were taken  
from Itoh et al. (1995) and consider general factors like different or rotating principal stress directions, full reversed loadings  
or step length influences. From Meggiolaro and de Castro (2014), 5 additional critical paths were extracted, addressing e. g. a  
275 90° phase shift or the influence of the mean stress.

Table 2 shows computational results of the  $f_{NP}$  test cases for the approaches according to Bishop (2000) and Meggiolaro and  
de Castro (2014) as well as the formulation proposed in this paper. These show that the derived method behaves in exactly the  
same way as the approach from Bishop (2000) for all load paths which are symmetric to the origin. Similar to Meggiolaro and  
de Castro (2014), it correctly predicts a nearly proportional stress path for test case 16 of  $f_{NP} = 0.054$ , where the formulation  
280 of Bishop (2000) recognises an ellipsis in the [Voigt-Mandel](#) notation around a mean value and computes the same value as for  
test case 15 ( $f_{NP} = 0.858$ ). This difference becomes also clear for the random loading centered in the origin (test case 20)  
compared to test case 19, where an offset was introduced. Test case 18 provokes the same problem for Bishop's approach  
(Bishop, 2000) considering the mean value but with the result that equation (2) only leads to one non-zero eigenvalue and  
thus to  $f_{NP} = 0$ , which represents proportional loading. However, this path is characterized by a 45° variation of the principal  
285 stress direction. For this stress path the method proposed in this work yields  $f_{NP} = 0.555$ , reflecting a similar value as the

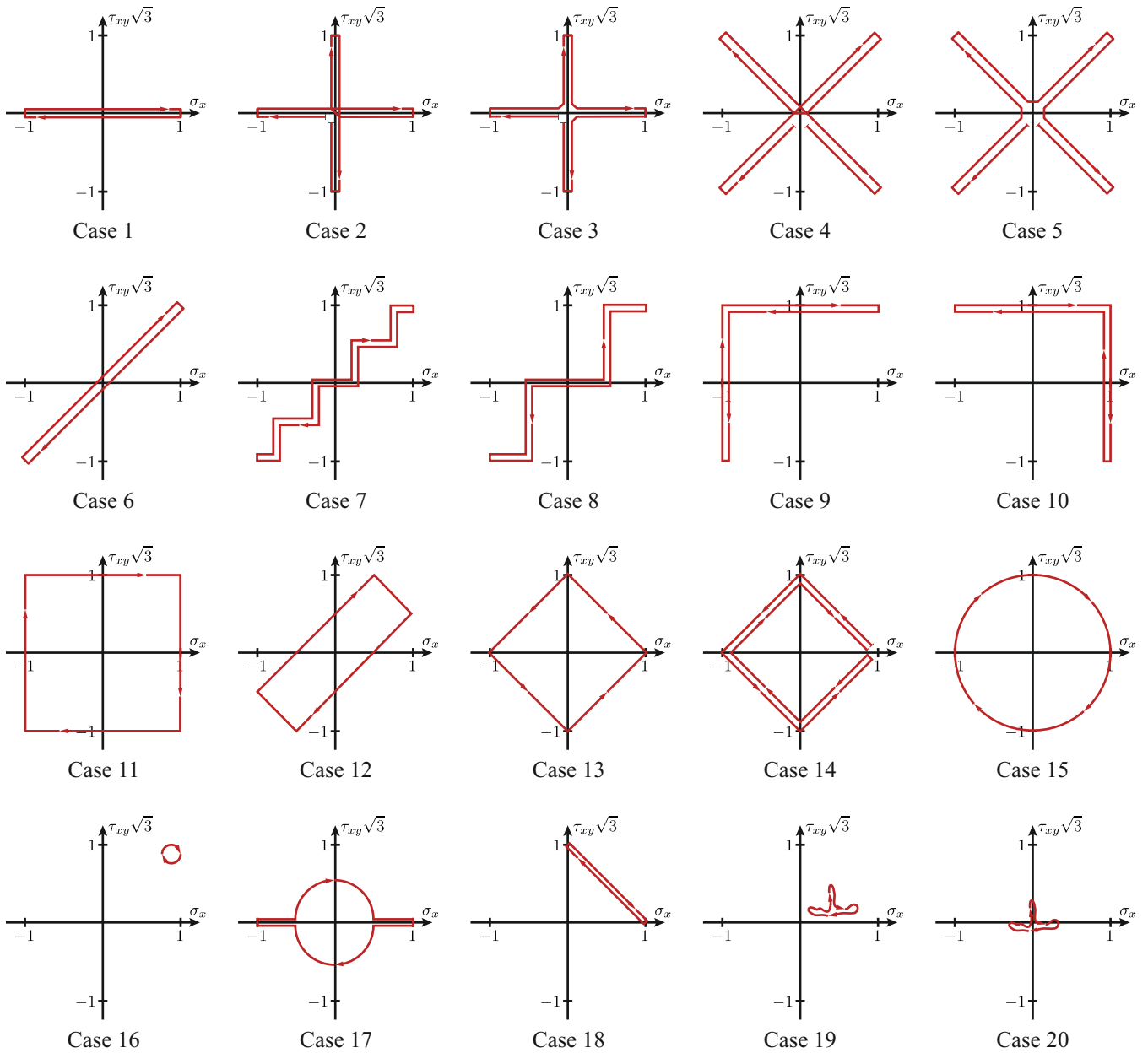


**Figure 2.** [Load history test cases used for comparison of the non-proportionality factor approaches, extracted and reproduced from Itoh et al. \(1995\) and Meggiolaro and de Castro \(2014\).](#)

approach of Meggiolaro and de Castro (2014). In general, the non-proportionality factor proposed in this paper computes the same values for stress paths without mean values as Bishop's approach (Bishop, 2000) and tends to results of the formulation of

**Table 2.** Comparison of the non-proportionality factors computed for the stress histories shown in Figure 2 according to Bishop (2000), Meggiolaro and de Castro (2014), and the approach proposed in this paper.

Test case	Bishop (2000)	Meggiolaro and de Castro (2014)	Proposed formulation
1	0.000	0.000	0.000
2	0.738	1.000	0.738
3	0.738	1.000	0.738
4	0.816	1.000	0.816
5	0.816	1.000	0.816
6	0.000	0.000	0.000
7	0.121	0.123	0.121
8	0.231	0.230	0.231
9	0.478	1.000	0.859
10	0.478	1.000	0.859
11	0.859	1.000	0.859
12	0.418	0.430	0.418
13	0.817	1.000	0.817
14	0.817	1.000	0.817
15	0.858	1.000	0.858
16	0.858	0.055	0.054
17	0.408	0.502	0.408
18	0.000	0.577	0.555
19	0.518	0.231	0.195
20	0.518	0.654	0.518

Meggiolaro and de Castro (2014) for non-zero mean values. However, there is still some discrepancy to Meggiolaro’s approach (Meggiolaro and de Castro, 2014) due to the different representation of the stress space.

#### 290 4 Application examples

The analysis of non-proportionality in fatigue stress histories for adhesive joints in wind turbine rotor blades is crucial for the understanding of the physical nature of fatigue damage and therefore for the choice of a reasonable method for the fatigue damage calculation. Therefore, three different blades were analysed in order to avoid blade-specific conclusions obtained from the study.

295 Two rotor blades were chosen to compare similar-sized blades, one from the DTU 10 MW reference turbine (Bak et al., 2013) with a length of 86 m, and the other one from the IWES IWT-7.5-164 reference turbine (Popko et al., 2018) with a length of 80 m. Additionally, the 20 m long demonstrator blade (Bätge, 2016) from the *SmartBlades2* project (Tessmer et al.,

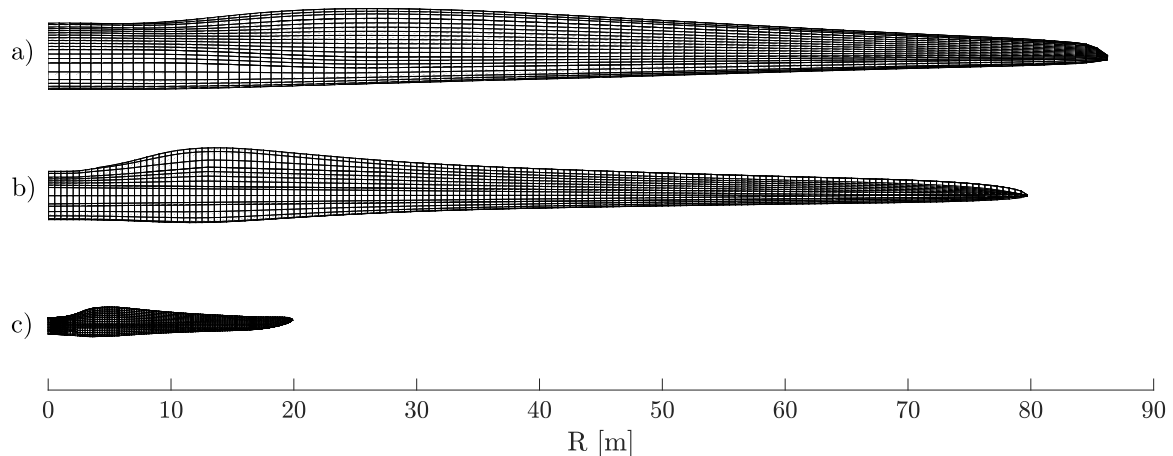


**Figure 3.** Finite element models of the three investigated rotor blades : a) DTU 10 MW (Bak et al., 2013), b) IWES IWT-7.5-164 (Popko et al., 2018), c) SB2-DemoBlade (Bätge, 2016)

2021), which is called *SB2-DemoBlade* in the following, is used to broaden the investigations to different blade sizes. The latter blade has a pre-sweep in the rotor area towards the trailing edge resulting in a geometric bend-twist coupling, i. e., the thrust  
 300 forces result in torsion introducing shear stresses in the trailing edge adhesive.

Finite element (FE) models of the selected blades were generated with the in-house tool MoCA (Model Creation and Analysis tool). The modeling strategy was validated in detail using the SB2-DemoBlade (Noever Castelos et al., 2022). Mesh convergence studies were carried out with respect to static deflections, natural frequencies, mode shapes, blade mass, and location of the center of gravity for all blades to ensure converged and reliable solutions. Figure 3 shows coarse versions of the  
 305 blade meshes (the used FE meshes were too fine for visualization) of all three blades, highlighting the size differences. Ansys was used as the FE solver. The post-processing, i. e. the calculation and analysis of non-proportionality factors, was executed using own routines in Matlab.

All composite components of the blades were represented by 4-noded shell elements. The trailing edge adhesive joints were modelled with 8-noded solid elements, see the detail view in Figure 4 exemplarily for the IWES IWT-7.5-164 blade. Since  
 310 the transitions from the root sections to the thin aerodynamic airfoils were different for the three blades (including the design of the trailing edge adhesive joints), the analyses were limited to the outboard regions of the blades at normalized radii of  $0.45 < r/R < 0.9$ , where  $r$  is the local radius and  $R$  is the rotor radius. Note that the radii are measured from the blade root, i.e., the hub radius is neglected. The FE meshes were further refined in the analysis regions in order to obtain better stress resolutions and stress convergence (local mesh refinement which is not displayed in the FE mesh images).

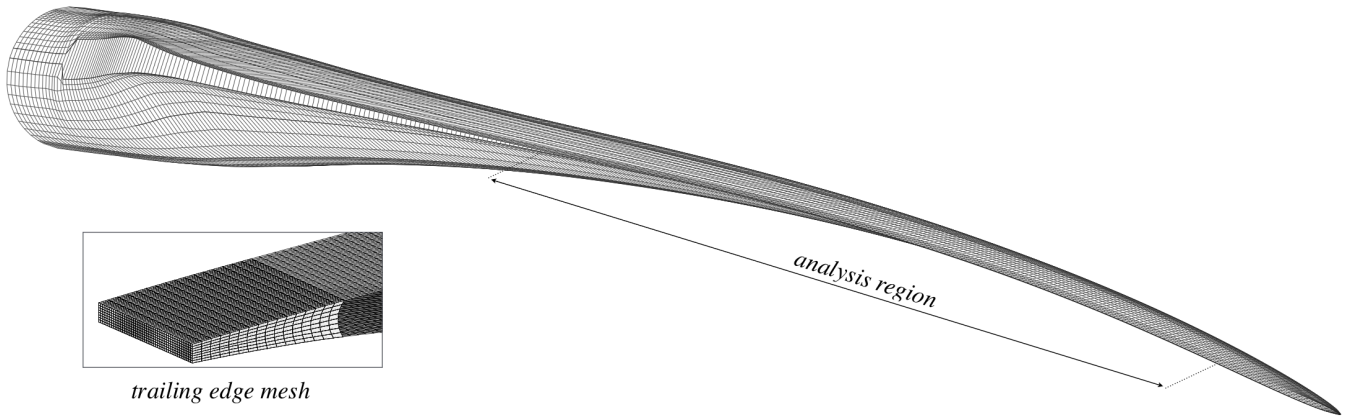


**Figure 4.** Visualization of the analysis region and a detailed view of the trailing edge FE mesh of the IWES-IWT-7.5 reference turbine blade.

## 315 5 Results and discussion

The non-proportionality of the adhesive joints was analysed on the basis of the fatigue load time series calculated for the design load case *power production* (DLC 1.2) according to the IEC standard 61400-1 [\(International Electrotechnical Commission, 2019\)](#). These load time series were translated to stress histories for each finite element representing the trailing edge adhesive joints according to the methodology described in [Noever Castelos and Balzani \(2016b\)](#) [\(Noever Castelos and Balzani, 2016b\)](#). The non-proportionality factors  $f_{NP}$  were then calculated according to the newly proposed formulation introduced in section 3.

### 5.1 Non-proportionality in trailing edge adhesive joints

In Figure 5, the maximum non-proportionality factors  $f_{NP,max}$  found in the trailing edge adhesive elements in each cross-section along the span of the blade are illustrated as a contour plot for all three blades. Therein, the normalized radii  $r/R$  are plotted on the  $x$  axes and the wind velocities  $v$  on the  $y$  axes. The colour scale is given on the left, and the corresponding Weibull frequency of occurrence distributions of the wind velocities,  $h_W$ , on the right.

Figure 5 (a) depicts the results for the DTU 10 MW reference blade. A generally low degree of non-proportionality can be observed with a global average of about  $f_{NP,max} = 0.2$ . In a region close to the blade tip ( $r/R > 0.85$ ), the local average reaches a maximum value of the non-proportionality factor of  $f_{NP,max} = 0.4$  for wind speeds of  $12 < v < 19$  m/s. When it comes to the contribution of fatigue damage (which is not evaluated in this paper), it is important to consider the frequency of occurrence of the wind velocity, as this will be used for the damage extrapolation in the assessment of the fatigue life. In the case of the DTU 10MW blade, an offshore Weibull distribution is used with a scaling factor of  $A = 10.2$  m/s and a shape factor of  $k = 2.2$ . In this case, the wind velocities resulting in higher non-proportionality factors ( $12 < v < 19$  m/s, see above), covers approximately 25 % of the year, whereas the lower wind velocities ( $4 < v < 11$  m/s) appear in 64 % of the year, but result in much lower  $f_{NP,max}$  values. However, the higher wind velocities are normally [linked-associated](#) with higher stress

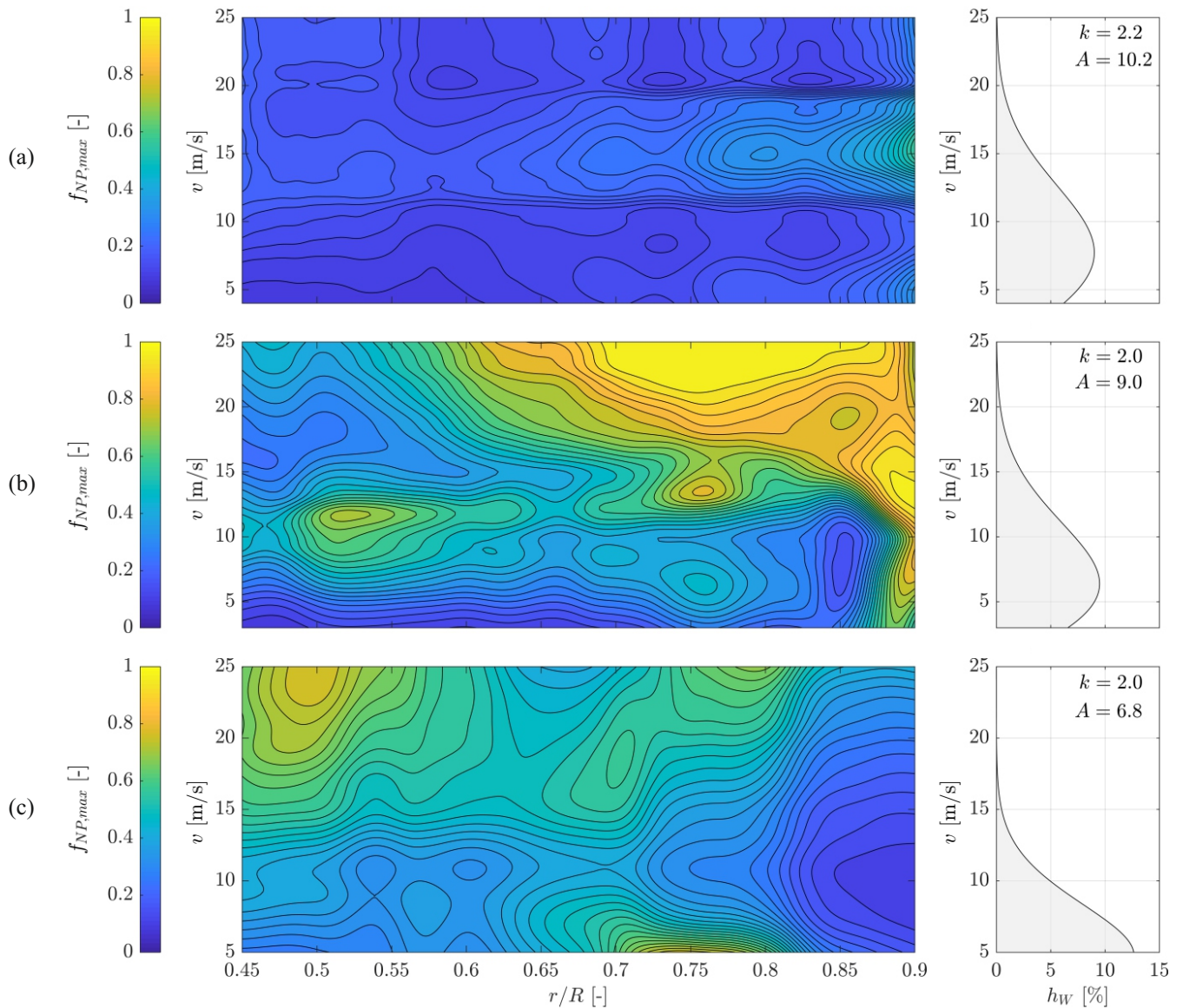


**Figure 5.** Contour plot of the non-proportionality factors as a function of the normalized radius  $r/R$  (on the  $x$  axis) and the wind velocity  $v$  (on the  $y$  axis): (a) DTU-10MW reference turbine blade (Bak et al., 2013); (b) IWES IWT-7.5-164 reference turbine blade (Popko et al., 2018); (c) SB2-DemoBlade (Bätge, 2016). Colour scale presented on the left, Weibull frequency of occurrence distribution of the wind velocity on the right.

335 amplitudes. The Hence, the non-proportionality is thus considered to may have a significant influence on the damage evolution, at least in the regions where higher degrees of non-proportionality are present.

Although the IWES 7.5 MW blade is similar in length, the design is qualitatively very different to the DTU blade, see also Figure 3. The distribution of the non-proportionality factor along the span of the blade and the wind velocities hence also appears very much different. The degree of non-proportionality generally reaches much higher values than that in the DTU blade, see Figure 5 (b). In general, the degree of non-proportionality increases with the radius and the wind velocity. However, there ~~is also a hot spot~~ are two hot spots at a normalized radius of  $0.5 < r/R < 0.55$  and a wind velocity of  $9 < v < 12$  m/s and ~~another one~~ at  $0.7 < r/R < 0.77$  and  $13 < v < 16$  m/s, respectively. The Weibull frequency of occurrence distribution is ~~one for~~ associated with a high wind speed near shore site (i.e.,  $A = 9.0$  m/s and  $k = 2.0$ ). Hence, the high non-proportionality is present also at wind speeds with non-negligible probability.

The SB2-DemoBlade is much shorter than the other two blades. It is a pretty stiff blade design, but includes a pre-sweep for geometrical bend-twist coupling. The contour plot of the non-proportionality factor is shown in Figure 5 (c). The non-proportionality is generally higher than in the DTU blade, but not as high as in the IWES blade. Two hot spots are present at high wind velocities ( $v > 18$  m/s) in two regions along the blade (i.e.,  $0.45 < r/R < 0.55$  and  $0.73 < r/R < 0.82$ ). The design site conditions for this blade ~~design is~~ are low wind speed and onshore, hence  $A = 6.8$  m/s and  $k = 2.0$ . The aforementioned Weibull parameters were derived from measurements of the field research validation site of NREL's CART3 turbine (Jager and Andreas, 1996) that the blade was designed for and set into operation for some time. Consequently, the wind velocity frequencies of occurrence are very low for the two non-proportionality hot spots. The non-proportionality at the aforementioned positions may thus be irrelevant for the fatigue assessment. However, there is a third hot spot at a radial position of  $0.68 < r/R < 0.8$  and a low wind speed of about 5 m/s. The frequency of occurrence of the wind speed in this location is very high, so the non-proportionality may affect the fatigue damage significantly here.

## 5.2 Correlation with stress time series

Figure 6 shows a representative excerpt (duration 50 s) of the stress time series in the trailing edge adhesive of all blades. A normalized radial position of  $r/R = 0.77$  and the wind speed with the highest frequency of occurrence are chosen exemplarily. The stress time series are plotted for the element with the highest  $f_{NP}$  factor for the considered cross-sections and wind speeds. Note that we neglected the outermost row of elements in order to ensure not to consider stresses close to singularities associated with geometric corners or discrete jumps of material properties. The stress results are calculated in the blade coordinate system according to DNV GL (2015), meaning that the  $z$  axis is pointing from the blade root to the blade tip, the  $y$  axis from the leading to the trailing edge, and the  $x$  axis from the pressure to the suction side. Hence,  $\sigma_x$  is the through-thickness normal stress in the adhesive,  $\sigma_y$  is the normal stress along the width of the adhesive,  $\sigma_z$  is the longitudinal normal stress, and  $\tau_{xy}$ ,  $\tau_{xz}$ , and  $\tau_{yz}$  are the in-plane and the transverse shear stresses, respectively.

The stress time series for the DTU blade is plotted in Figure 6 (a). It can be seen that the longitudinal stress  $\sigma_z$  is dominating the time series with an amplitude of approximately 1.5 MPa, a mean stress of approximately 1 MPa and a 1/revolution frequency. The mean stress is caused by the torque resulting in power output of the turbine. The oscillation is due to a high edgewise bending moment originating from the blade mass in rotation. The other stresses have negligible amplitudes and mean stresses. The dominating longitudinal normal stress corresponds to the small non-proportionality factor of  $f_{NP} = 0.159$  (i.e.,

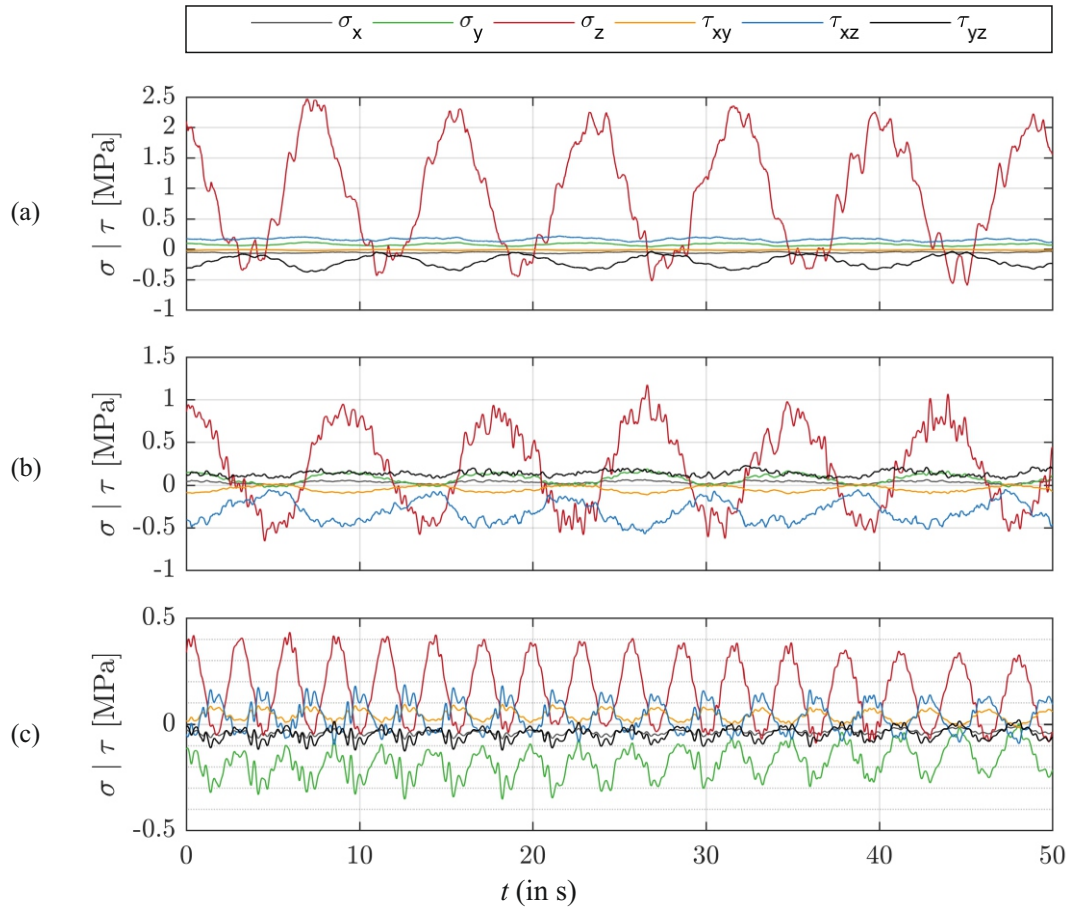


**Figure 6.** Stress histories of the finite element in the trailing edge adhesive joints with the highest non-proportionality at a normalized radial position of  $r/R = 0.77$  for all investigated blades, related to the blade coordinate system according to DNV GL (2015): (a) DTU 10 MW reference blade,  $v = 8$  m/s,  $f_{NP} = 0.159$ ; (b) IWES IWT-7.5-164 reference blade,  $v = 7$  m/s,  $f_{NP} = 0.465$ ; (c) SB2 Demo blade,  $v = 5$  m/s,  $f_{NP} = 0.766$ .

almost proportional stress history) in the trailing edge adhesive displayed in Figure 5 (a), as this results in a very pronounced RMOI in  $z$  direction and far smaller RMOIs in the other directions.

Figure 6 (b) presents the stress time series for the IWES blade. The major excitation frequency is again 1/revolution and is of the same magnitude as that in the DTU blade, as the blade size is and the tip speed ratio are very similar. The longitudinal normal stress is still the dominant stress component. The amplitude is much lower compared to the DTU blade (approximately 0.75 MPa), as well as the mean stress (approximately 0.25 MPa). The reason is the different design philosophy expressed in the general blade shape (see Figure 3) resulting in a different mass distribution and a stiffer trailing edge girder reducing the strain and consequently the stress in the trailing edge adhesive. The through-thickness transverse shear stress  $\tau_{xz}$  is remarkably higher than in the DTU blade, and also remarkably higher than all other stress components, but still significantly smaller than

380 the longitudinal normal stress. However, it does contribute to the non-proportionality factor, especially since there is a  $90^\circ$  phase shift with respect to  $\sigma_z$ , see also test case 15 in section 3. Consequently, the non-proportionality factor is  $f_{NP} = 0.465$ , which is about three times higher than that in the DTU blade, see also Figure 5 (b).

The stress time series of the SB2-DemoBlade is presented in Figure 6 (c). It can be seen that the governing 1/revolution excitation frequency is much higher compared to the DTU and the IWES blades. This is due to the much smaller rotor diameter  
385 (tip speed ratio is a bit smaller, but the rotor diameter is about one fourth). The longitudinal normal stress  $\sigma_z$  has the highest amplitude of about 0.25 MPa and mean stress of approximately 0.15 MPa. In contrast to the DTU and the IWES blades, other stress components are much higher. E.g., the normal stress in width direction,  $\sigma_y$ , is about half as much as  $\sigma_z$ , which is not negligible. Moreover, the inplane and transverse shear stress in thickness direction, namely  $\tau_{xy}$  and  $\tau_{xz}$ , respectively, contribute notably with respect to amplitude. It is worth mentioning that the major part of the longitudinal normal stress is deterministic  
390 in nature, i.e.i.e., it shows a low amount of temporal variations from a sinusoidal signal. The other stress components have a much higher fluctuation, i.e.i.e., a higher stochastic content. The stress history for this blade results in a higher degree of non-proportionality expressed by a high non-proportionality factor at the exemplary location and wind speed of  $f_{NP} = 0.766$ . The reason for that is the higher contributions of stress components apart from the longitudinal stress. Some of these are in phase. E.g., the normal stresses  $\sigma_y$  and  $\sigma_z$  have the peaks and valleys at the same time. This normally results in a proportional  
395 stress history. However, the higher variability of  $\sigma_y$  contributes to non-proportionality. Other stress components, e.g.e.g., the shear stresses  $\tau_{xy}$  and  $\tau_{xz}$ , respectively, show a  $90^\circ$  phase shift to the aforementioned normal stresses, which naturally results in non-proportionality. The phase shift is due to the different excitation: The normal stresses  $\sigma_y$  and  $\sigma_z$  are governed by the blade mass in rotation, resulting in peaks and valleys when the blade is in 3 o'clock and 9 o'clock azimutal-azimuthal position. The shear stresses  $\tau_{xy}$  and  $\tau_{xz}$ , however, are influenced by asymmetries in the wind field, namely the wind shear, resulting in  
400 peaks and valleys at azimutal-azimuthal positions of 6 and 12 o'clock, respectively.

One might be forgiven for assuming that investigating the non-proportionality degree in the adhesive is an unnecessary exercise, given that transverse cracks are a common occurrence in operating turbines (Ataya and Ahmed, 2013; Rosemeier et al., 2022b). This is evidently due to the dominant longitudinal normal stress. In such a scenario, the search for the critical plane is rendered unnecessary, as its existence is already known. This is currently the case since adhesive joints in rotor blades are  
405 often designed for shear stress transfer only. To circumvent the formation of transverse cracks, it would be prudent to reinforce the trailing edge laminate, for instance, through the incorporation of additional unidirectional material. As a result, the strains in the trailing edge and, consequently, the longitudinal normal stress in the adhesive would be decreased. A reduction in the longitudinal normal stress would result in an increase in the degree of non-proportionality, with the relative contribution of other stress components also rising. While there is a possibility that thermal residual stresses may become a critical issue if  
410 the trailing edge is excessively stiff (Rosemeier et al., 2022a), it should be feasible to identify an optimal solution through a process of compromise. It should be noted that the present study did not account for thermal residual stresses, which introduces an error in the stress histories (Rosemeier et al., 2019b, a). However, as recently highlighted by Kuhn (2023), the bi-axial combination of a constant stress in one direction and a cyclic stress in the other direction results in non-proportionality. This finding can be readily extended to a multi-axial stress state. The constant thermal residual stress in the longitudinal direction

415 (Rosemeier et al., 2022b), superimposed by the cyclic shear stress components, would thus result in a further increase in the degree of non-proportionality. Therefore, the simplification is conservative with respect to the non-proportionality factor. It can be concluded that considering non-proportional fatigue should be of even greater importance in properly designed rotor blades (meaning, designed for shear stress transfer and longitudinal strain) when thermal residual stresses are taken into account, in light of the results presented in this study.

### 420 5.3 Weighted mean non-proportionality

Up to here, the non-proportionality factor was given for each wind velocity. However, it is necessary to evaluate the degree of ~~non-proportionality~~ non-proportionality for the entire service life of the wind turbine including all possible wind velocities. A weighted mean value of the ~~non-proportionality~~ non-proportionality factor is thus calculated employing the wind velocity frequency of occurrence distribution function as a weighting factor. Introducing the cut-in and cut-out wind velocities by  $v_{in}$  and  $v_{out}$  and an integer number  $i$  identifying a wind speed bin, the weighted mean of the non-proportionality factor,  $\bar{f}_{NP}$ , is given by the relationship

$$\bar{f}_{NP} = \frac{\sum_{i=v_{in}}^{v_{out}} f_{NPi} h_{Wi}}{\sum_{i=v_{in}}^{v_{out}} h_{Wi}} . \quad (9)$$

Herein,  $f_{NPi}$  is the non-proportionality factor for the given wind speed bin  $i$  and  $h_{Wi}$  is the frequency of occurrence of said wind speed bin according to the Weibull distribution functions given in Figure 5.

430 Figure 7 shows  $\bar{f}_{NP}$  distributed across the cross-section of the trailing edge adhesive joint at a radial position of  $r/R = 0.77$  for all three blades, corresponding to the radial position of the stress history excerpt given in Figure 6. The cross-sectional views show ~~a part~~ parts of the suction side shells ~~on the top~~ and a part of (at the top) and the pressure side shells ~~on the bottom~~ (at the top). The trailing edge is on the right, respectively. As already concluded from the contour plots of Figure 5 and the stress histories in Figure 6, the DTU 10 MW blade shows the lowest and the SB2-DemoBlade the highest degree of non-proportionality. However, for all blades the distribution in the cross-section is qualitatively similar. The inner face of the adhesive joint has the highest degree of non-proportionality which is decreasing towards the trailing edge. This is due to the increasing distance to the principal bending axis and consequentially increasing longitudinal normal stresses  $\sigma_z$  from edge wise bending. The dominance of  $\sigma_z$  is thus increasing towards the trailing edge, making the stress histories more proportional.

440 It is important to exercise caution when interpreting the stresses in the corners of the adhesive, as it is widely acknowledged that stresses do not converge with the mesh density in such singularities (geometric sharp corner and/or sudden jump in material properties in the interface between adhesive and shell laminates). Given that the non-proportionality factor is a direct consequence of the stress state, it is similarly prudent to exercise caution when considering the non-proportionality factor in the corners. However, in the subsequent analysis, the non-proportionality factor in the outermost elements of the adhesive were excluded from the results, ensuring that the conclusions are valid and not affected by spurious stress components.

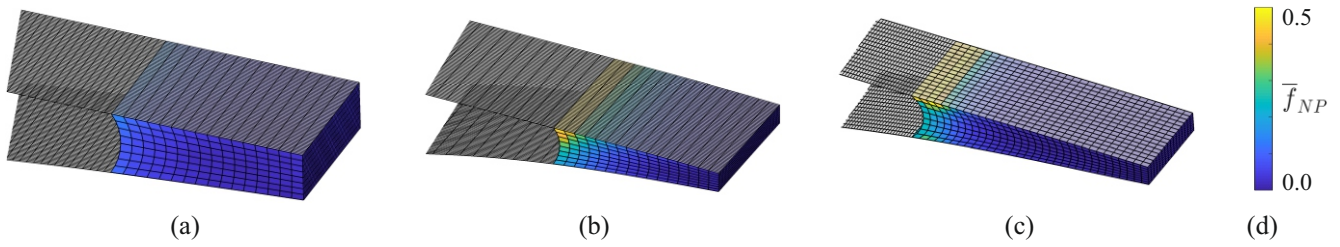


**Figure 7.** Contour plots of the weighted mean non-proportionality factor  $\bar{f}_{NP}$  in the trailing edge adhesive for all three blades (cut-out with the visible cross-section at a radial position of  $r/R = 0.77$ ): (a) DTU blade; (b) IWES blade; (c) SB2-DemoBlade; (d) color code.

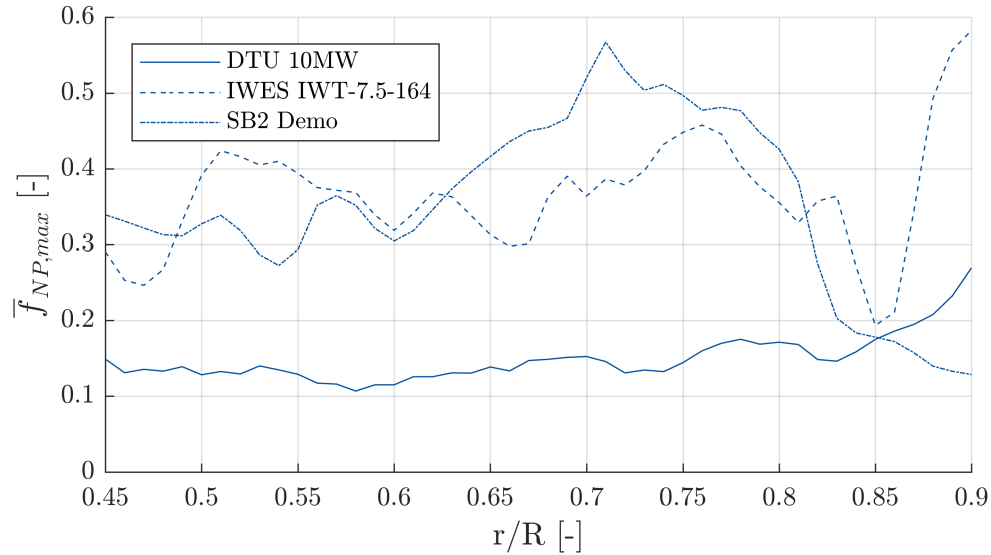


**Figure 8.** Maximum weighted mean non-proportionality factor  $\bar{f}_{NP,max}$  in the trailing edge adhesive joint plotted as a function of the normalized radial position  $r/R$  for all three blades.

445 The maximum weighted mean non-proportionality factor in each cross-section,  $\bar{f}_{NP,max}$ , is plotted as a function of the  
normalized radial position for all three blades in Figure 8. In the DTU blade, the degree of non-proportionality factor is  
very low, see the explanations above. It is more or less constant at a value of  $0.11 < \bar{f}_{NP,max} < 0.18$  along the blade, but  
increases towards the blade tip to its maximum of about 0.28. The IWES blade, which has a similar length, has moderate  
non-proportionality values of  $0.3 < \bar{f}_{NP,max} < 0.4$  with a more distinct variability along the blade. The SB2-DemoBlade has  
450 a peak of non-proportionality at a radial position of  $0.6 < r/R < 0.8$  with a maximum value of about 0.58. In this region,  
the non-proportionality factor is higher than in the other blades, whereas at smaller and larger radial positions, the degree of  
non-proportionality is lower than that in the IWES blade, and close to the tip also lower than that of the DTU blade. The large  
blades (DTU and IWES blade) behave somewhat similar close to the tip, where the degree of non-proportionality is increasing.  
Contrarily, the SB2-DemoBlade's non-proportionality is decreasing towards the blade tip. [Generally speaking, it can be seen](#)

455 that ~~in general, the distribution~~ the distributions of the maximum weighted mean non-proportionality factor along the blade is ~~very significantly~~ different for the three blades analyzed in this work.

## 6 Conclusions

In this paper, a non-proportionality factor was proposed that ~~helps~~ serves to quantify the degree of non-proportionality in a fatigue stress time series. Two different formulations from literature were combined. The non-proportionality factor was  
460 evaluated for 20 test cases on which the new formulation was benchmarked against other formulations. The agreement was excellent for those test cases where no difference was expected. It was further shown that the non-proportionality calculated with the new formulation is independent of a mean stress (which is an important feature) and accounts for hydrostatic pressure states. The new formulation is thus an improvement for materials that are sensitive to the presence of hydrostatic pressure in fatigue, as is the case for an epoxy-based adhesive investigated in this paper.

465 The non-proportionality factor was then applied to evaluate the degree of non-proportionality in trailing edge adhesive joints of three different rotor blades, two of which having a similar blade size and the third one being smaller and being equipped with a pre-sweep in the rotor plane. The characteristics of the degrees of non-proportionalities were analyzed in detail and were correlated with excerpts of the load time series.

Generally, the non-proportionality degrees in the three blades are very different. It is thus difficult (or impossible) to draw  
470 general conclusions on the degree of non-proportionality. The higher degree of non-proportionality in the SB-DemoBlade could be triggered by the geometrical bend-twist coupling originated by the pre-sweep in the rotor area. The DTU and IWES blades are numerical blade models that were developed for the research community. They may thus not be representative for a commercial blade designed for operation in the field. The SB2-DemoBlade, however, was designed for field testing of geometrical bend-twist coupling. The structural design was thus executed on a much higher level of detail, but due to the small  
475 size may not be representative for modern utility-scale wind turbines.

A correlation between the degree of non-proportionality and the blade size was not substantiated. The reason is that the stress response in a blade depends on a large variety of influencing factors, such as the choice of the fatigue analysis methodology (global equivalent stress vs. critical plane approach), the choice of the underlying equivalent stress criteria, the quality of the material database, the general design policy of the blade designer, the design targets with respect to aero-elastic performance  
480 and cost, the risks the designer is willing to accept, the overall turbine concept, the dynamic response not only of the blades but also of the entire turbine, different inflow conditions of small and large rotor diameters, etc. Hence, the degree of non-proportionality in a rotor blade has to be analyzed for each turbine individually.

However, it was shown that non-proportionality is generally present in each of the analysed blades. While it was very low in the DTU 10 MW blade, the degree of non-proportionality was significant in the IWES 7.5 MW blade and in the  
485 SB2-DemoBlade. A common finding for all three blades was that the longitudinal normal stress was the predominant stress component. ~~The~~, which agrees well with the observation of transverse cracks in operating wind turbines. A major goal in blade design ~~with respect to a trailing edge adhesive joint~~ should thus be to avoid excessive longitudinal strain and stress.

This cannot be realized by increasing the bondline width, which is the usual design parameter for adhesive joints, but by increasing the stiffness of the trailing edge girder to reduce the longitudinal strain. When doing this, care must be taken not to implement excessively high stiffness in order to avoid damages from thermal residual stresses. However, if the longitudinal stress is reduced in this way, the other stress components not affected by the stiffening of the trailing edge girder  $\bar{\sigma}$  will become more significant and the degree of non-proportionality will increase.

The distribution of the non-proportionality factor in the cross-section plane was similar in all cases and increased from the trailing edge towards the inner face corner on the suction side. It was observed that a dominating longitudinal normal stress, which can appear in real blades, reduces the degree of non-proportionality (which is also the reason for the cross-sectional distribution of the non-proportionality factor).

It was shown in literature that the choice of a suitable fatigue analysis framework depends on the degree of non-proportionality. For proportional stress histories, a global equivalent stress approach gives reasonable and accurate fatigue damage estimates. However, if there is a lot of non-proportionality involved, the critical plane approach needs to be utilized (which is computationally very intense), because the error of the global equivalent stress approach increases with the level of non-proportionality, and the error is not necessarily conservative.

The non-proportionality factor as proposed in this paper can be utilized to quantify the degree of non-proportionality in rotor blade adhesive joints, and it can be adapted for other materials and sub-structures as well. The blade designer is then able to select an appropriate fatigue analysis methodology, e. g., the critical plane approach, only for spots with a high degree of non-proportionality and the. On the contrary, the global equivalent stress approach can be applied elsewhere. As the wrong choice of the fatigue analysis method can be non-conservative, the non-proportionality factor can thus serve to improve the overall structural reliability of wind turbine rotor blades.

Further research is necessary to find a threshold above which non-proportionality needs to be considered. Future work will have to clarify in how far the non-proportionality factor can be utilized as a decision-making metric in choosing an appropriate fatigue analysis procedure, finding the best compromise between accuracy and computational cost before actually carrying out the fatigue analysis.

*Code and data availability.* For legal reasons, code and data cannot be shared at this stage. The authors will try to provide code and data needed for reproduction of the findings by the time of final publication in case the manuscript will be accepted.

*Author contributions.* CB wrote the paper, did a part of the literature research, and provided scientific guidance and supervision to PNC in all project phases. PNC did the rest of the literature research, derived the equations, implemented pre- and postprocessing scripts in Matlab, carried out the simulations, prepared figures, and internally reviewed the manuscript.

*Competing interests.* The authors do not have competing interests.

*Disclaimer.* The information in this paper is provided as is and no guarantee or warranty is given that the information is fit for any particular purpose. The user thereof uses the information at its sole risk and liability.

520 *Acknowledgements.* This research was funded by the Deutsche Forschungsgemeinschaft (DFG, German Research Foundation) as part of the Collaborative Research Center 1463 ‘Integrated Design and Operation Methodology for Offshore Megastructures’ (SFB1463 – Project ID 434502799) and by the German Federal Ministry for Economic Affairs and Climate Actions (BMWK) of Germany as part of the coordinated research projects ‘SmartBlades2’ (Project ID 0324032C) and ‘ReliaBlade’ (Project ID 0324335B). The authors acknowledge the financial support.

## 525 References

- Adams, R. D.: Adhesive bonding: Science, technology and applications, CRC Press, Boca Raton, FL and Cambridge, 2005.
- Amos Gilat, Robert K. Goldberg, and Gary D. Roberts: Strain Rate Sensitivity of Epoxy Resin in Tensile and Shear Loading, NASA, Springfield, 2005.
- Anes, V., Reis, L., Li, B., and de Freitas, M.: New approach to evaluate non-proportionality in multiaxial loading conditions, *Fatigue & Fracture of Engineering Materials & Structures*, 37, 2014.
- Antoniou, A., Rosemeier, M., Tazefidan, K., Krimmer, A., and Wolken-Möhlmann, G.: Impact of site-specific thermal residual stress on the fatigue of wind-turbine blades, *AIAA Journal*, 58, 4781–4793, <https://doi.org/10.2514/1.J059388>, 2020.
- Antoniou, A. E., Vespermann, M. M., Sayer, F., and Krimmer, A.: Life prediction analysis of thick adhesive bond lines under variable amplitude fatigue loading, in: *Proceedings of the 18th European Conference on Composite Materials (ECCM18)*, June 24–28, Athens, Greece, pp. 1–8, 2018.
- Ataya, S. and Ahmed, M. M.: Damages of wind turbine blade trailing edge: Forms, location, and root causes, *Engineering Failure Analysis*, 35, 480–488, <https://doi.org/https://doi.org/10.1016/j.engfailanal.2013.05.011>, special issue on ICEFA V- Part 1, 2013.
- Bak, C., Zahle, F., Bitsche, R., Kim, T., Yde, A., Henriksen, L. C., Natarajan, A., and Hansen, M. H.: Description of the DTU 10 MW Reference Wind Turbine, Tech. rep., DTU Wind Energy, 2013.
- Balzani, C. and Gebauer, J.: Impact of shell structure stiffness on aero-structural coupling in wind turbine rotor blades, *IOP Conference Series: Materials Science and Engineering*, 1293, 012 025, <https://doi.org/10.1088/1757-899X/1293/1/012025>, 2023.
- Bätge, M.: Design of a 20 m blade for the demonstration turbine (Deliverables 1.2.6.2/1.2.6.3), *Schlussbericht Projekt SmartBlades*, 2016.
- Beber, V. C., Fernandes, P., Schneider, B., Brede, M., and Mayer, B.: Fatigue lifetime prediction of adhesively bonded joints: An investigation of the influence of material model and multiaxiality, *International Journal of Adhesion and Adhesives*, 78, 240–247, 2017.
- Beltrami, E.: Sulle condizioni di resistenza dei corpi elastici, *Il Nuovo Cimento*, 18, 145–155, 1885.
- Bishop, J. E.: Characterizing the non-proportional and out-of-phase extent of tensor paths, *Fatigue & Fracture of Engineering Materials & Structures*, 23, 1019–1103, 2000.
- Boopathi, K., Mishnaevsky Jr., L., Sumantraa, B., Premkumar, S. A., Thamodharan, K., and Balaraman, K.: Failure mechanisms of wind turbine blades in India: Climatic, regional, and seasonal variability, *Wind Energy*, 25, 968–979, <https://doi.org/10.1002/we.2706>, 2022.
- Chen, X., Berring, P., Madsen, S. H., Branner, K., and Semenov, S.: Understanding progressive failure mechanisms of a wind turbine blade trailing edge section through subcomponent tests and nonlinear FE analysis, *Composite Structures*, 214, 422–438, <https://doi.org/10.1016/j.compstruct.2019.02.024>, 2019a.
- Chen, X., Haselbach, P. U., Branner, K., and Madsen, S. H.: Effects of different material failures and surface contact on structural response of trailing edge sections in composite wind turbine blades, *Composite Structures*, 226, 111 306, <https://doi.org/10.1016/j.compstruct.2019.111306>, 2019b.
- Christensen, R. M.: A two-property yield, failure (fracture) criterion for homogeneous, isotropic materials, *Journal of Engineering Materials and Technology*, 126, 45–52, 2004.
- de Castro, J. T. P. and Meggiolaro, M. A.: *Fatigue Design Techniques Under Real Service Loads, Volume II – Low-Cycle and Multiaxial Fatigue*, CreateSpace Independent Publishing Platform, 1st edn., 2016.
- Deng, Q.-Y., Zhu, S.-P., He, J.-C., Li, X.-K., and Carpinteri, A.: Multiaxial fatigue under variable amplitude loadings: review and solutions, *International Journal of Structural Integrity*, 13, 349–393, 2022.

- Deng, Q.-Y., Zhu, S.-P., Niu, X., Lesiuk, G., Macek, W., and Wang, Q.: Load path sensitivity and multiaxial fatigue life prediction of metals under non-proportional loadings, *International Journal of Fatigue*, 166, 107 281, 2023.
- DNV GL: DNVGL-ST-0376 – Rotor blades for wind turbines, 2015.
- 565 Downing, S. D. and Socie, D. F.: Simple rainflow counting algorithms, *International Journal of Fatigue*, 4, 31–40, 1982.
- Drucker, D. C. and Prager, W.: Soil mechanics and plastic analysis or limit design, *Quarterly of Applied Mathematics*, 10, 157–165, 1952.
- Eder, M., Bitsche, R., Nielsen, M., and Branner, K.: A practical approach to fracture analysis at the trailing edge of wind turbine rotor blades, *Wind Energy*, 17, 483–497, <https://doi.org/10.1002/we.1591>, 2014.
- Eder, M. A. and Bitsche, R. D.: Fracture analysis of adhesive joints in wind turbine blades, *Wind Energy*, 18, 1007–1022, 570 <https://doi.org/10.1002/we.1744>, 2015.
- Eder, M. A., Semenov, S., and Sala, M.: Multiaxial Stress Based High Cycle Fatigue Model for Adhesive Joint Interfaces, in: *Computational and Experimental Simulations in Engineering – Proceedings of ICCES2019, Mechanisms and Machine Science*, vol 75, edited by Okada, H. and Atluri, S., pp. 621–632, Springer, Cham., 2020.
- Endo, T., Mitsunaga, K., Takahashi, K., Kobayashi, K., and Matsuishi, M.: Damage evaluation of metals for random or varying loading – 575 three aspects of rain flow method, *Mechanical Behavior of Materials*, 1, 371–380, 1974.
- Fan, J., Vassilopoulos, A. P., and Michaud, V.: Mode I fracture of thick adhesively bonded GFRP composite joints for wind turbine rotor blades, *Composite Structures*, 327, 117 705, <https://doi.org/10.1016/j.compstruct.2023.117705>, 2024.
- Fatemi, A. and Shamsaei, N.: Multiaxial fatigue: An overview and some approximation models for life estimation, *International Journal of Fatigue*, 33, 948–958, 2011.
- 580 Haselbach, P. U.: An advanced structural trailing edge modelling method for wind turbine blades, *Composite Structures*, 180, 521–530, <https://doi.org/10.1016/j.compstruct.2017.08.029>, 2017.
- Haselbach, P. U. and Branner, K.: Effect of Trailing Edge Damage on Full-Scale Wind Turbine Blade Failure, in: *Proceedings of the 20th International Conference on Composite Materials (ICCM20)*, Copenhagen, Denmark, 2015.
- Haselbach, P. U. and Branner, K.: Initiation of trailing edge failure in full-scale wind turbine blade test, *Engineering Fracture Mechanics*, 585 162, 136–154, <https://doi.org/10.1016/j.engfracmech.2016.04.041>, 2016.
- Haselbach, P. U., Eder, M. A., and Belloni, F.: A comprehensive investigation of trailing edge damage in a wind turbine rotor blade, *Wind Energy*, 19, 1871–1888, <https://doi.org/10.1002/we.1956>, 2016.
- Hu, W., Choi, K. K., Zhupanska, O., and Buchholz, J. H. J.: Integrating variable wind load, aerodynamic, and structural analyses towards accurate fatigue life prediction in composite wind turbine blades, *Structural and Multidisciplinary Optimization*, 53, 375–394, 590 <https://doi.org/10.1007/s00158-015-1338-5>, 2016.
- Hu, W., Zhao, W., Wang, Y., Liu, Z., Cheng, J., and Tan, J.: Design optimization of composite wind turbine blades considering tortuous lightning strike and non-proportional multi-axial fatigue damage, *Engineering Optimization*, 52, 1868–1886, <https://doi.org/10.1080/0305215X.2019.1690649>, 2020.
- Hu, Y., Xia, Z., and Ellyin, F.: Deformation behavior of an epoxy resin subject to multiaxial loadings. Part I: Experimental investigations, 595 *Polymer Engineering and Science*, 43, 721–733, 2003.
- International Electrotechnical Commission: Wind energy generation system – Part 1: Design requirements, *International Standard No. 61400-1:2019*, 2019.
- Itoh, T., Sakane, M., Ohnami, M., and Socie, D. F.: Nonproportional Low Cycle Fatigue Criterion for Type 304 Stainless Steel, *Journal of Engineering Materials and Technology*, 117, 285–292, 1995.

- 600 Itoh, T., Sakane, M., and Ohsuga, K.: Multiaxial low cycle fatigue life under non-proportional loading, *International Journal of Pressure Vessels and Piping*, 110, 50–56, 2013.
- Jager, D. and Andreas, A.: NREL National Wind Technology Center (NWTC): M2 Tower; Boulder, Colorado (Data), 1996.
- Kanazawa, K., Miller, K. J., and Brown, M. W.: Cyclic deformation of 1% Cr-Mo-V Steel under out-of-phase loads, *Fatigue & Fracture of Engineering Materials & Structures*, 2, 217–228, 1979.
- 605 Katsaprakakis, D. A., Papadakis, N., and Ntintakis, I.: A Comprehensive Analysis of Wind Turbine Blade Damage, *Energies*, 14, 5974, <https://doi.org/10.3390/en14185974>, 2021.
- Kuhn, M.: Non-proportional fatigue by example of fiber-reinforced rotor blade adhesive, phdthesis, Leibniz University Hannover, Institute for Wind Energy Systems, <https://doi.org/10.15488/15770>, 2023.
- Kuhn, M., Manousides, N., Antoniou, A., and Balzani, C.: Effects of non-proportionality and tension–compression asymmetry on the fatigue  
610 life prediction of equivalent stress criteria, *Fatigue & Fracture of Engineering Materials & Structures*, 46, 3161–3178, 2023.
- Lahuerta, F., Koorn, N., and Smisshaert, D.: Wind turbine blade trailing edge failure assessment with sub-component test on static and fatigue load conditions, *Composite Structures*, 204, 755–766, <https://doi.org/10.1016/j.compstruct.2018.07.112>, 2018.
- Lee, Y.-L. and Tjhung, T.: Metal fatigue analysis handbook – practical problem-solving techniques for computer-aided engineering, chap. 3 – Rainflow Cycle Counting Techniques, pp. 89–114, Elsevier Inc., 2012.
- 615 Liu, X., Lu, C., Liang, S., Godbole, A., and Chen, Y.: Vibration-induced aerodynamic loads on large horizontal axis wind turbine blades, *Applied Energy*, 185, 1109–1119, 2017.
- Manolas, D. I., Riziotis, V. A., and Voutsinas, S. G.: Assessing the Importance of Geometric Nonlinear Effects in the Prediction of Wind Turbine Blade Loads, *Journal of Computational and Nonlinear Dynamics*, 10, 041 008, 1–15, 2015.
- Meggiolaro, M. A. and de Castro, J. T. P.: An improved multiaxial rainflow algorithm for non-proportional stress or strain histories – Part I:  
620 Enclosing surface methods, *International Journal of Fatigue*, 42, 217–226, 2012.
- Meggiolaro, M. A. and de Castro, J. T. P.: Prediction of non-proportionality factors of multiaxial histories using the Moment Of Inertia method, *International Journal of Fatigue*, 61, 151–159, 2014.
- Meggiolaro, M. A., de Castro, J. T. P., and Wu, H.: On the use of tensor paths to estimate the nonproportionality factor of multiaxial stress or strain histories under free-surface conditions, *Acta Mechanica*, 227, 3087–3100, 2016.
- 625 Noever Castelos, P. and Balzani, C.: On the impact of multi-axial stress states on trailing edge bondlines in wind turbine rotor blades, *Journal of Physics: Conference Series*, 753, 062 002, 2016a.
- Noever Castelos, P. and Balzani, C.: The impact of geometric non-linearities on the fatigue analysis of trailing edge bond lines in wind turbine rotor blades, *Journal of Physics: Conference Series*, 749, 012 009, 2016b.
- Noever Castelos, P., Haller, B., and Balzani, C.: Validation of a modeling methodology for wind turbine rotor blades based on a full-scale  
630 blade test, *Wind Energy Science*, 7, 105–127, 2022.
- Popko, W., Thomas, P., Sevinc, A., Rosemeier, M., Bätge, M., Braun, R., Meng, F., Horte, D., Balzani, C., Bleich, O., Daniele, E., Stoevesandt, B., Wentingmann, M., Polman, J. D., Leimeister, M., Schürmann, B., and Reuter, A.: Reference Wind Turbine IWT-7.5-164 Rev 4, Tech. rep., Fraunhofer Institute for Wind Energy Systems IWES, Bremerhaven, Germany, 2018.
- Raghava, R., Caddell, R. M., and Yeh, G. S. Y.: The macroscopic yield behaviour of polymers, *Journal of Materials Science*, 8, 225–232,  
635 1973.
- Rosemeier, M., Alexander, K., Bardenhagen, A., and Antoniou, A.: Tunneling crack initiation in trailing-edge bond lines of wind-turbine blades, *AIAA Journal*, 57, 5462–5474, <https://doi.org/10.2514/1.J058179>, 2019a.

- Rosemeier, M., Krimmer, A., Bardenhagen, A., and Antoniou, A.: Fatigue impact of mechanical and thermal residual stresses on the trailing edge bond line of wind turbine blades, in: AIAA Scitech 2019 Forum, January 7-11, 2019, San Diego, California, USA, pp. 1–13, 640 <https://doi.org/10.2514/6.2019-0246>, 2019b.
- Rosemeier, M., Gebauer, T., and Antoniou, A.: A practical approach for the peel stress prediction in the trailing-edge adhesive joint of wind turbine blades, IOP Conference Series: Materials Science and Engineering, 942, 012026, <https://doi.org/10.1088/1757-899X/942/1/012026>, 2020.
- Rosemeier, M., Gebauer, T., and Antoniou, A.: Sub-component versus full wind turbine blade structure: Influence of manufacture-induced 645 thermal residual stresses on crack initiation in adhesive joints, in: 20th European Conference on Composite Materials (ECCM20), June 26-30, Lausanne, Switzerland, <https://doi.org/10.5281/zenodo.6786885>, 2022a.
- Rosemeier, M., Melcher, D., Krimmer, A., Wroblewski, W., and Antoniou, A.: Validation of crack initiation model by means of cyclic full-scale blade test, Journal of Physics: Conference Series, 2265, 032045, <https://doi.org/10.1088/1742-6596/2265/3/032045>, 2022b.
- Rubiella, C., Hessabi, C. A., and Fallah, A. S.: State of the art in fatigue modelling of composite wind turbine blades, International Journal 650 of Fatigue, 117, 230–245, <https://doi.org/10.1016/j.ijfatigue.2018.07.031>, 2018.
- Rychlik, I.: A new definition of the rainflow cycle counting method, International Journal of Fatigue, 9, 119–121, 1987.
- Schleicher, F.: Der Spannungszustand an der Fließgrenze (Plastizitätsbedingung), Journal of Applied Mathematics and Mechanics / Zeitschrift für Angewandte Mathematik und Mechanik (ZAMM), 6, 199–216, 1926.
- Socie, D. F. and Marquis, G. B.: Multiaxial fatigue, Society of Automotive Engineers, Warrendale, Pa., 2000.
- 655 Sonsino, C. M.: Multiaxial fatigue life response depending on proportionality grade between normal and shear strains/stresses and material ductility, International Journal of Fatigue, 135, 105468, 2020.
- Stassi-D’Alia, F.: Flow and fracture of materials according to a new limiting condition of yielding, Meccanica, 2, 178–195, 1967.
- Stephens, R. I., Fatemi, A., Stephens, R. R., and Fuchs, H. O.: Metal fatigue in engineering, Wiley, New York, 2nd edn., 2001.
- Söker, H.: Advances in Wind Turbine Blade Design and Materials, chap. 2 – Loads on wind turbine blades, pp. 29–58, Woodhead Publishing 660 Limited, Cambridge, UK, 2013.
- Tessmer, J., Montano Rejas, Z. M., Rose, M., Daniele, E., Stoevesandt, B., Riemenschneider, J., Hölling, M., and Balzani, C.: SmartBlades2 – Bau, Test und Weiterentwicklung intelligenter Rotorblätter, Final Report (in German), 2021.
- Teßmer, J., Icpinar, C., Sevinc, A., Daniele, E., Riemenschneider, J., Hölling, M., and Balzani, C.: Smart Blades – Entwicklung und Konstruktion intelligenter Rotorblätter, Final Report (in German), 2016.
- 665 van Kuik, G. and Peinke, J., eds.: Long-term Research Challenges in Wind Energy - A Research Agenda by the European Academy of Wind Energy, vol. 6 of *Research Topics in Wind Energy*, Springer International Publishing Switzerland, 2016.
- van Kuik, G. A. M., Peinke, J., Nijssen, R., Lekou, D., Mann, J., Sørensen, J. N., Ferreira, C., van Wingerden, J. W., Schlipf, D., Gebraad, P., Polinder, H., Abrahamson, A., van Bussel, G. J. W., Sørensen, J. D., Tavner, P., Bottasso, C. L., Muskulus, M., Matha, D., Lindeboom, H. J., Degraer, S., Kramer, O., Lehnhoff, S., Sonnenschein, M., Sørensen, P. E., Künneke, R. W., Morthorst, P. E., and Skytte, K.: Long- 670 term research challenges in wind energy – a research agenda by the European Academy of Wind Energy, Wind Energy Science, 1, 1–39, 2016.
- Vassilopoulos, A. P.: Fatigue life prediction of wind turbine blade composite materials, in: Advances in Wind Turbine Blade Design and Materials, edited by Brøndsted, P. and Nijssen, R. P., Woodhead Publishing Series in Energy, chap. 8, pp. 251–297, Woodhead Publishing, ISBN 978-0-85709-426-1, <https://doi.org/10.1533/9780857097286.2.251>, 2013.

- 675 Veers, P., Dykes, K., Lantz, E., Barth, S., Bottasso, C. L., Carlson, O., Clifton, A., Green, J., Green, P., Holttinen, H., Laird, D., Lehtomäki, V., Lundquist, J. K., Manwell, J., Marquis, M., Meneveau, C., Moriarty, P., Munduate, X., Muskulus, M., Naughton, J., Pao, L., Paquette, J., Peinke, J., Robertson, A., Rodrigo, J. S., Sempreviva, A. M., Smith, J. C., Tuohy, A., and Wisser, R.: Grand challenges in the science of wind energy, *Science*, 366, eaau2027, <https://doi.org/10.1126/science.aau2027>, 2019.
- 680 Veers, P., Bottasso, C. L., Manuel, L., Naughton, J., Pao, L., Paquette, J., Robertson, A., Robinson, M., Ananthan, S., Barlas, T., Bianchini, A., Bredmose, H., Horcas, S. G., Keller, J., Madsen, H. A., Manwell, J., Moriarty, P., Nolet, S., and Rinker, J.: Grand challenges in the design, manufacture, and operation of future wind turbine systems, *Wind Energy Science*, 8, 1071–1131, <https://doi.org/10.5194/wes-8-1071-2023>, 2023.
- von Mises, R.: Mechanik der festen Körper im plastisch-deformablen Zustand, *Nachrichten von der Gesellschaft der Wissenschaften zu Göttingen, Mathematisch-Physikalische Klasse*, 4, 582–592, 1913.
- 685 Wang, J., Huang, X., Wei, C., Zhang, L., Li, C., and Liu, W.: Failure analysis at trailing edge of a wind turbine blade through subcomponent test, *Engineering Failure Analysis*, 130, 105596, <https://doi.org/10.1016/j.engfailanal.2021.105596>, 2021.
- Wentingmann, M., Noever-Castelos, P., and Balzani, C.: An adaptive algorithm to accelerate the critical plane identification for multi-axial fatigue criteria, in: *Proceedings of the 6th European Conference on Computational Mechanics and the 7th European Conference on Computational Fluid Dynamics*, edited by Owen, R., de Borst, R., Reese, J., and Pearce, C., pp. 3745–3754, CIMNE, 2018.
- 690 Wentingmann, M., Manousides, N., Antoniou, A., and Balzani, C.: Yield surface derivation for a structural adhesive based on multi-axial experiments, *Polymer Testing*, 113, 107648, 2022.
- White, D. L. and Musial, W. D.: The Effect of Load Phase Angle on Wind Turbine Blade Fatigue Damage, *Journal of Solar Energy Engineering*, 126, 1050–1059, 2004.
- Wu, H., Qi, L., Qian, J., Cao, H., Shi, K., and Xu, J.: Experimental research on the compression failure of wind turbine blade trailing edge structure, *The Journal of Adhesion*, 99, 1488–1507, <https://doi.org/10.1080/00218464.2022.2126313>, 2023.
- 695 Zouain, N., Mamiya, E. N., and Comes, F.: Using enclosing ellipsoids in multi-axial fatigue strength criteria, *European Journal of Mechanics - A/Solids*, 25, 51–71, 2006.